Report No. __Y/DA-7745__

MATERIALS FOR HIGH-TEMPERATURE
HYDROGEN-FLUORINE ENVIRONMENTS

C. E. Holcombe
L. Kovach
G. W. Weber

February 21, 1978

UNION CARBIDE

OAK RIDGE Y-12 PLANT

OAK RIDGE, TENNESSEE

19980309 281

Ltr. No. 78F-0309-067 TRW 62
AO 3443

UNION CARBIDE

UNION CARBIDE CORPORATION SLL 80 629
COPY 1

NUCLEAR DIVISION

LASER
CL, M

P. O. BOX Y, OAK RIDGE, TENNESSEE 37830

March 9, 1978

Air Force Weapons Laboratory
Attention: Capt. N. Pchelkin
Chemical Laser Branch
Kirtland Air Force Base, New Mexico 87115

Department of Defense
Defense Advanced Research Project Agency
Attention: Capt. H. Winsor
Materials Science Section
1400 Wilson Blvd
Arlington, Virginia 22209

Gentlemen:

<u>Advanced Low-Heat-Loss Nozzle Research Program</u>

Enclosed is a report describing the results of work conducted during
the period from October 1, 1977, to February 15, 1978, on AFWL
Project Order 78-002. This document covers investigations conducted
to complete cylindrical sample testing, initial design of the con-
figuration testing assembly, new materials developments, and initial
heat transfer studies.

Please direct any comments you might have regarding this report to
Dr. G. W. Weber.

Very truly yours,

W. R. Martin, Director
Development Division

GWW:tf

Attachment: Y/DA-7745

Distribution:

Same as listed in report

U4025

MATERIALS FOR HIGH-TEMPERATURE
HYDROGEN-FLUORINE ENVIRONMENTS

C. E. Holcombe
L. Kovach
G. W. Weber

Y-12 Development Division

February 21, 1978

CONTENT

SUMMARY

This report is a continuation of the testing of candidate materials for use as uncooled nozzles for a hydrogen-fluorine laser system currently being developed by the Defense Advanced Research Projects Agency (DARPA), the Air Force Weapons Laboratory (AFWL), and the Missile Research and Development Command (MIRADCOM).

Data from 36 recent runs in the hydrogen-fluorine (HF) test facility have been collected, with emphasis on the current primary candidates for the project—beryllia (BeO), magnesia (MgO), alumina (Al_2O_3), and lanthanum hexaboride (LaB_6). Metallics, including nickel (Ni-270), nickel and titanium aluminides (NiAl and TiAl), scandium (Sc), and yttrium (Y), were also tested. Single crystals of Al_2O_3 (sapphire) and MgO were examined. Also included were lanthanum chromite ($LaCrO_3$), silicon nitride (Si_3N_4), and lanthanum-silicon oxynitride ($La_2O_3 \cdot Si_3N_4$). All specimens were tested to failure in order to determine the surface temperature of emergence of rapid reaction, or the surface temperature which cannot be equalled or exceeded without significant weight and dimensional changes.

In previous studies at Y-12, the upper use-temperature for near-zero corrosion appeared to be determined by the stability and characteristics of the protective fluoride layer. When this layer melts, sublimes or otherwise loses integrity, protection for the substrate deteriorates, with the degree of deterioration at that point determined by the heat of reaction, viscosity of the fluoride layer, and its vapor pressure. The adherence, porosity, and degree of microcracking of the layer are other determining factors of the corrosion rate. Whether a single or polycrystalline sample is used appears to have little effect on film protection (based on Al_2O_3 or MgO results).

The current ranking of best performers for a low-heat-loss, uncooled laser nozzle, in order of decreasing performance is:

$$LaB_6 \ [1750K]^+ > \ La_2O_3 \cdot Si_3N_4 \ [1600K] > Sc \approx LaCrO_3 \approx Ni \approx NiAl \approx Y$$

$$[1450K] \ > MgO \ [1300K] \ > \ BeO \approx Al_2O_3 \approx TiAl \ [1200K] \ > C \ [1000K].$$

LaB_6 is approximately 300K "better" than metallics, which would also have low strengths and low creep resistance at $\geq$ 1400K making it difficult to maintain dimensional tolerances. Thus, the practical upper use-temperatures of metallics may be well below their approximate zero-reaction temperatures.

$^+$Approximate zero-reaction temperature rounded to nearest 50K.

After ten runs on a single LaB_6 sample with 87 minutes at flame temperatures > 1700K, the cumulative weight loss was less than 0.6% with virtually no detectable dimensional changes. Even after "failure", the corrosion was not catastrophic as the fluoride layer appeared viscous and relatively protective, as only 0.96% cumulative weight loss occurred and sample configuration was retained. A further experiment demonstrated the thermal shock resistance of the material by direct heating of LaB_6 in a 3000K flame and subsequent rapid cooling. There was no indication of thermal shock cracking.

In addition to HF testing, a materials test chamber assembly has been designed and constructed. Initial operation will begin shortly, followed by testing of C, MgO, Al_2O_3, and LaB_6 two and three-dimensional configurations.

INTRODUCTION

The HF (hydrogen-fluoride) chemical laser requires high-temperature, hydrogen-fluoride molecules that are excited to an elevated vibrational state and allowed rapid expansion.

The principal nozzle material previously considered was nickel—requiring internal cooling and thus special machining for coolant flow, as well as creating reduced lasing efficiencies from the high energy losses through the flowing coolant. Therefore, interest has developed in uncooled nozzle materials in the activity entitled "Advanced Low-Heat-Loss Nozzle Research Program."

In previous reports[1,2] the design, construction, and operation of the HF test facility has been outlined, including the results of the initial screening phase of the program and the testing of over 100 samples. The initial materials selection criteria was also previously discussed.

This report covers the continuation of materials testing, particularly relating to the determination of the relative upper use-temperature for near-zero corrosion. Also, the preliminary design and construction of a materials test chamber assembly is presented.

SECTION I. EXPERIMENTAL: DESIGN AND FABRICATION OF A MATERIAL
TEST CHAMBER ASSEMBLY

Upon completion of the screening phase encompassing the testing of 1-inch-
diameter cylindrical specimens, a new testing phase will be conducted. In
addition to the chemical and temperature effects, the erosion effects of
the HF torch gases on test materials will be evaluated. Initial exploratory
runs will be conducted in a test chamber design as shown in Figure 1.

Selected materials will be fabricated as test plates, drilled with a pre-
scribed number of holes, and fastened to the bottom of the chamber.
Initial runs will be made with 36 drilled holes, 1.016 mm diameter, set
in a square array on 5.59 mm centers. A sight port with a sapphire or
calcium fluoride window will permit observation of the flame and its effect
on the test plate. The temperature of the test plate will be determined
with a 1.0-mm-diameter thermocouple, inserted from the side, and pyrometer
readings taken through the sight port. A pressure tap connected to a
pressure gage will monitor the pressure in the chamber. Maximum pressure
should not exceed approximately 5 psig. Provision has also been made in
the chamber design to reduce the distance between the nozzle tip and the
test plate as desired. This may be required if gas flow rates need to be
reduced. The deflection ring, shown in Figure 1, is designed to reduce eddy
flows and the possibility of accelerated corner corrosion.

The chamber will be threaded onto the existing Monel nozzle assembly within
the large Monel test chamber to permit easy installation and removal.
Initially, the chamber will be fabricated from ATJ graphite because of its
low cost, easy machinability, and low corrosion rate in a fluorine environ-
ment at temperatures below 700°C.

The nozzle currently in use for specimen testing was also redesigned. Instead
of a tapered coaxial converging flame, the new design will provide a broader
flame front to equalize temperatures and exposure on the broader sample
plates.

SECTION II. EXPERIMENTAL: OPERATION OF MATERIALS TESTING FACILITY

A. MATERIALS TESTING RUNS

Thirteen different materials were investigated with 36 separate runs
in the HF test facility. For nonmetallic specimens, a nickel sample
holder was used. For metallic, either a nickel or a graphite (thermal
conductivities are approximately equal to or above 1073K) sample
holder was used with a thin ($\sim$ 1.5 mm) alumina disc placed between
the metal and sample holder to ensure relative thermal isolation.
For rod specimens (supplied by TRW), a nickel holder was used and the
flame contacted the rod on an edge, splitting the flame. The ends of
the rod were isolated thermally by placing oxide grit ($\leq$ 1.5 mm grains
of Al_2O_3 or MgO), of the material being tested between the nickel
support and the rod.

Existing Monel
Nozzle Assembly

ATJ Graphite

Sapphire Window

1"

Sliding
Fit

5"

1" dia

42°

Deflection
Ring, Removable

Sight Port

1 5/16" Ref

Add
Dowel Pin

2 1/2" Dia. Ref

Test Plate
0.150" Thick
to be drilled with
36 holes — 0.040" dia.
on 0.220" centers
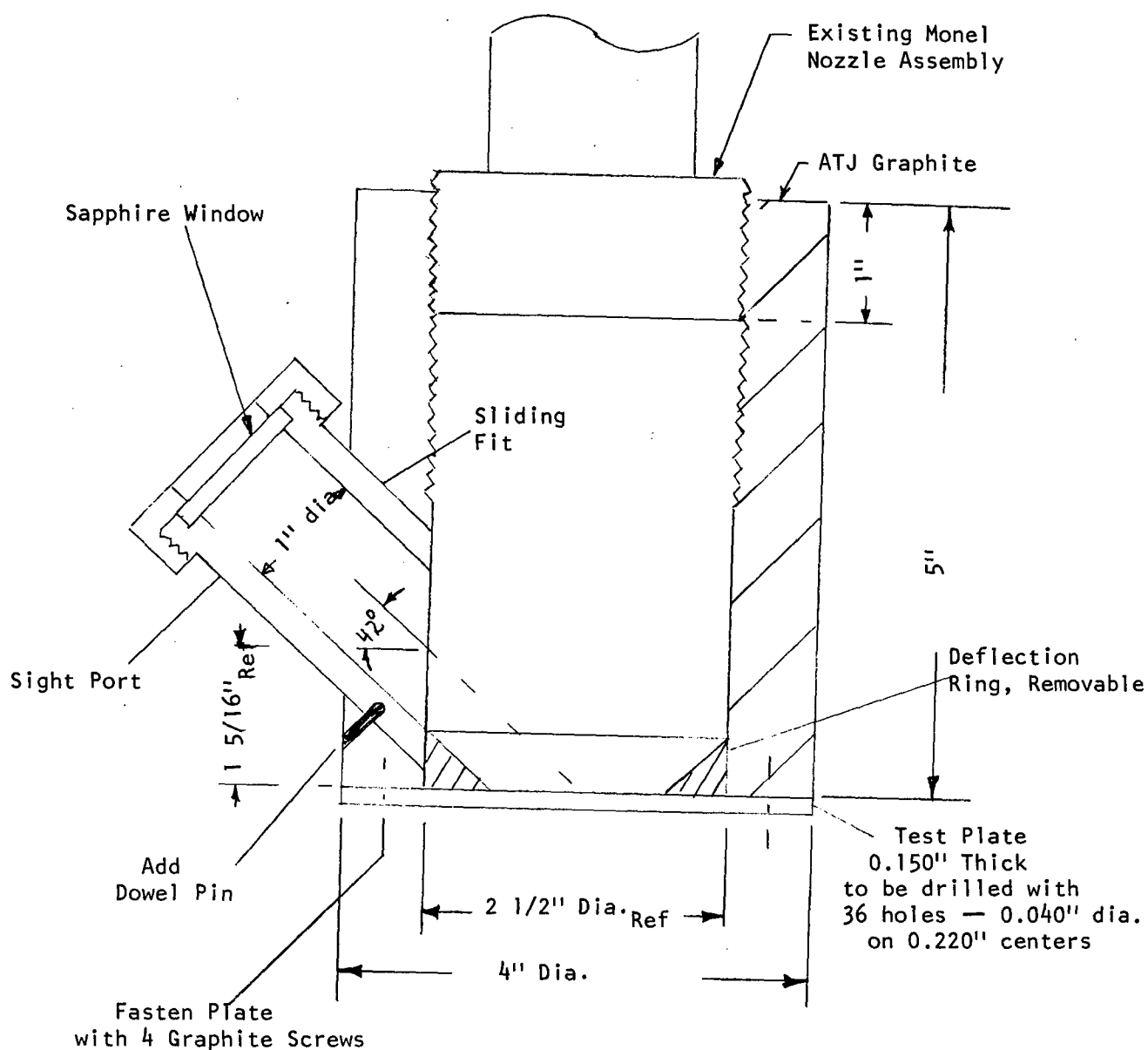
4" Dia.

Fasten Plate
with 4 Graphite Screws

Figure 1.   MATERIAL TEST CHAMBER ASSEMBLY.

A programmed heating cycle was used for nonmetallic specimens (except for one LaB_6 and one $LaCrO_3$ sample) to minimize the possibility of thermal shock, as previously discussed.[1,2] Because of the improved performance, it was found necessary when testing certain materials to use higher flame temperatures than previously employed.[1,2] This was necessary to reach the surface temperatures at which failure occurs. Characteristically, these materials had high thermal conductivities and high thermal resistances. Although not strictly correct, a linear extrapolation of an existing theoretical flame temperatures plot from 1400K to 2400K for various helium, $2F_2/H_2$ mixtures, was used to attain temperatures ranging from 2400K to 3000K. Recent computer calculations have indicated that these extrapolated values were in error at higher temperatures and necessary changes in the run data presented in Appendices I and II have been made accordingly. In the most extreme case, the calculated flame temperature was determined to be 2853K instead of the predicted 3015K. In only one instance (Run HF-102 on LaB_6) was it found necessary to use a flame estimated to be in excess of 3000K. This was effected by decreasing the fluorine/hydrogen ratio from 2 to 1.2.

Run data presenting gas flows, theoretical flame temperatures, run cycle times, and recorded temperatures are presented in Appendix I. A change has been made in the data presentation. The temperature profile of the test chamber, previously measured with four thermocouples, is no longer reported. It is felt this data is not significant in our current investigations.

A summary of the run data, any dimensional and weight changes in the test specimens, plus visual observations are presented in Appendix II.

B. TEMPERATURE MEASUREMENTS AND THERMOCOUPLE EXPERIMENTS

The experiments have been monitored with both a manual and an automatic pyrometer. Pyrometer readings required, from calibration studies, a +15 to +25K correction (depending upon temperature) for the combined 3-mm-thick sapphire and 12.7-mm-thick quartz windows in the view port. A recent recalibration showed approximately no change in the calibration in the period covered by this report. The manual pyrometer readings utilized a mirror, which requires an additional temperature correction of +20K. The manual pyrometer permitted temperature readings as low as 1050K, while the automatic pyrometer began recording at 1138K. Slightly higher temperature readings normally resulted with the manual pyrometer because of the ability of the operator to selectively read the hotter areas on the specimen and discriminate from interfering gases being released from some samples. The automatic pyrometer, however, remains in a fixed attitude and averages the light emitted from the center of the specimen with a large reticle spot without regard for local anomalies and interference.

Uncertainty typically exists concerning surface temperatures determined by optical pyrometry, because of nonblackbody emissivity corrections. Further uncertainties arise because of the thin, possibly opaque, fluoride layer. In an effort to define true surface temperatures, further thermocouple experiments (as described previously[2]) were conducted with alumina and are planned with LaB_6, MgO, Ni-270, NiAl, and C. In these experiments, four nickel-sheathed, Pt-Pt/10 Rh thermocouples, 1.02 mm in diameter are placed into $\sim$ 1.5 mm dia. holes drilled in the typical 2.54-cm-dia., 1.27-cm-high cylinder. One thermocouple (#4) is very slightly ($\sim$ 1 mm) off-center, 6.6 mm (0.26 in) down from the top surface and another (#2) is 6.4 mm from the axis, 1.0 mm down from the top surface. The fourth thermocouple (#1) is 6.4 mm from the axis of the disc contacting the bottom surface. The thermocouples were monitored with a multipoint recorder capable of making ten measurements per minute for each thermocouple. During these runs (HF-130, HF-131, HF-132), both manual and automatic pyrometer readings were taken along with visual observations.

Two of the alumina runs (HF-130 and HF-131) were designed to maintain surface temperatures below those previously found to result in significant corrosion. The other run (HF-132) was designed to exceed the failure point. Further discussion of these runs may be found in Section III.B.3.

C. BERYLLIUM OXIDE TESTING RUNS

In the present operation of the facility, exhaust gases from the test chamber are discharged directly to the plume of the building ventilation stack. Because of the toxicity of finely divided Be compounds, it was necessary to meet specific industrial hygiene requirements to permit testing of BeO in this device. A stainless steel filter unit with a porous Monel element having 4 ft^2 of filter area and a removal rating of 100% for 1.0 μm size particles was installed in the 2-inch exhaust line. During the specimen testing runs, the filter performed satisfactorily, and there was no observable differential pressure.

Upon completion of the runs, the test chamber was determined to be highly contaminated with Be. However, the contamination in the exhaust piping adjacent to the filter and at the filter was found to be below acceptable levels. After a complete cleaning of the chamber with TF Freon and water and additional contamination tests, the equipment was deemed acceptable to permit resumption of normal operations.

SECTION III. RESULTS AND DISCUSSION

A. GENERAL DISCUSSION OF TEST RESULTS

The materials used in the high-temperature hydrogen fluoride tests are characterized by the data presented in Tables 1 and 2.* Most

---

*Note that SiC is characterized in Tables 1 and 2 since the data were not yet determined at the issue date of the previous report.[2]

Table 1

IMPURITY LEVEL INFORMATION

Materials	Impurities (wt % level in parentheses) Determined at a Detection Level $\geq$ 0.1 wt %	Comments
BeO (Y-12)	None detected	Spark source mass spectrographic analysis (MS) indicated > 99.99% pure; contains 390 wppm Li or 0.22 wt % Li_2O
BeO (Nat'l Beryllia Berlox K-150)	Mg (0.15), Si (0.2)	MS indicated > 99.54% pure; 0.08 wt % Al, probably clay-bonded
MgO Single Crystal	None detected	No impurities > 35 wppm, vendor certification (VC)
Sapphire Single Crystal (Al_2O_3)	None detected	MS indicated > 99.93% pure
Al_2O_3 (Coors)	Si (0.1)	
Sc_2O_3	Ta (< 0.15), Cs (< 0.6), Rb (0.2), P (< 1), Cd (1.5), U (< 0.3)	Emission Spectrographic Analysis (ES)
$LaCrO_3$	Ta (< 0.15), Cs (< 0.6), Rb (< 0.15), P (< 1), Th (< 0.3)	ES
SiC	Ta (< 0.15), Al (5), Cs (< 0.6), Rb (< 0.15), P (< 1), Ti (0.15), B (0.15), U (< 0.3)	ES; $\sim$ 5% Al as a hot-pressing aid
LaB_6	None detected	MS indicated > 99.84% pure
Si_3N_4 (nominal 5 wt % MgO)	Mg (5), Ta (< 0.15), Al (0.3), Cs (< 0.6), Rb (< 0.15), P (< 1), Ca (0.15)	ES
$La_2O_3 \cdot Si_3N_4$	Ta (< 0.15), Cs (< 0.6), Rb (< 0.15), P (< 1), Th (< 0.3)	ES

Table 2

PHYSICAL PROPERTY DATA

Materials	Bulk Density[3] (g/cm^3)	Real Density[3] (g/cm^3)	Open Porosity[3] (%)
BeO (Y-12)	3.00	3.02	0.6
BeO (Berlox)	2.87	2.87	0.1
MgO Single Crystal	3.60	3.60	0
Sapphire (Al_2O_3) Single Crystal	3.99	3.99	0
Al_2O_3 (Coors)	3.91	3.91	0
Sc_2O_3	3.43	3.76	8.9
$LaCrO_3$[1]	6.08	6.26	2.9
SiC	2.95	2.95	0.1
LaB_6	4.56	4.57	0.2
Si_3N_4 (MgO doped)[2]	3.16	3.19	0.9
$La_2O_3 \cdot Si_3N_4$[1]	3.75	4.70	20.3

[1]X-ray diffraction (XRD) indicated single phase

[2]XRD indicated major phase = β - Si_3N_4; intermediate phase = α - Si_3N_4

[3]Determined by mercury porosimeter

samples were purchased as hot-pressed cylinders, nominally > 99% pure, > 90% dense. Sapphire and magnesia single crystals in the typical cylindrical shape were also obtained. Lanthanum chromite ($LaCrO_3$), a candidate material for magnetohydrodynamic (MHD) generator channels, was purchased as a pressed-and-sintered cylinder. The silicon nitride materials (Si_3N_4 and $La_2O_3 \cdot Si_3N_4$) were hot pressed at Y-12.

The testing results are presented in detail in Appendix II. Only for Sc_2O_3 did catastrophic thermal shock failure prohibit obtaining any surface temperature information. Since the Sc_2O_3 sample was > 90% dense, it appears that Group IIIB oxides (also Y_2O_3) have such poor thermal shock resistance that they are unsuitable for this application. For rather porous Y_2O_3 samples, such cracking was previously considered to result from YF_3 vapor-pressure buildup in the pore blockage. Testing of a near-100% dense Y_2O_3 specimen is planned to attempt to verify the cause of such behavior.

Lanthanum chromite, $LaCrO_3$, while not reacting rapidly with $2F_2/H_2$, forms a very thick fluoride film. This film measured 0.029 inch thick on the top, 0.031 inch thick on the side of the cylinder near the top, and is readily flaked off. The film was identified as LaF_3 by X-ray diffraction. This indicates that the chromium fluorides (probably CrF_2 and CrF_3) volatilize. Since some melting of the film occurred, possibly a eutectic LaF_3/CrF_2 occurs first, causing some flow before CrF_2 vaporizes. The porous nature of the residual LaF_3 film probably depends on the atomic packing characteristics of the substrate and the number and size of the atoms which react and volatilize. The atomic density (atoms/cc) of the atoms removed by fluorination compared to the atomic density of residual (nonvolatile) atoms should determine the relative density (and thus protection from further reaction) of the fluoride layer that forms. In the case of $LaCrO_3$, the LaF_3 layer that forms is too porous to be very protective and thus considerable corrosion occurs. It should be noted that the material appears to have excellent thermal shock resistance since it withstood, with no apparent cracking, direct heating with a 2400K flame followed by subsequent rapid cooling. $LaCrO_3$ is also not water reactive.

The comparable maximum surface temperature for near-zero corrosion determined for twelve different materials is shown in Table 3. Test results for specific materials will be discussed later in the report. Note that emissivities of 0.4 are assumed for nonmetallic specimens and 0.5 for metallic specimens. While this is arbitrary, it does indicate maximum surface temperatures for there would be some emissivity correction. Oxide emissivities are typically in the 0.2-0.5 range, while a graybody (0.5) is a fair estimate for metals.

Considering 1400K as a lower maximum surface temperature for candidate materials, only LaB_6, $La_2O_3 \cdot Si_3N_4$, Sc, $LaCrO_3$, Ni, NiAl, and Y would be included. Because of its poor film characteristics, $LaCrO_3$ would probably be eliminated.

Table 3

MATERIAL PERFORMANCE IN HIGH-TEMPERATURE HF ENVIRONMENTS

Material	Maximum Surface Temperature[1] (K)	Assumed Film Emissivity (ϵ)	Assumed Emissivity Correction[2] (K)	Max. Surface Temp. Including Assumed Emissivity Correction (K)	Remarks
BeO(Y-12), HF-134	1158	0.4	62	1220	mp BeF_2 = 825-1075K; mp Be-O-F = 1025K
BeO (Berlox), HF-133	1093	0.4	53	1146	
MgO Single Crystal, HF-137	1241	0.4	70	1311	Rapid rise of surface temperature to 1464K (ϵ included); mp MgF_2 = 1536K; mp MgF_2-MgO = 1487K
MgO, HF-74	1248	0.4	71	1319	Rapid rise of surface temperature to 1560K (ϵ included)
MgO-3%Y_2O_3(TRW), HF-116	<< 1410	0.4	90	<< 1476	Rod specimen; reaction rate was too rapid for accurate temperature determination
Sapphire Single Crystal, HF-121	1126	0.4	57	1183	Sublimation point of AlF_3 = 1550K
Al_2O_3 (Coors), HF-132	1145	-	-	1145	From top thermocouple
Al_2O_3 (Coors), HF-135	1163	0.4	62	1225	
Al_2O_3-0.5%Y_2O_3 (TRW), HF-114	<< 1390	0.4	88	<< 1478	Rod specimen; reaction rate was too rapid for accurate temperature determination

Table 3 (Cont'd)

MATERIAL PERFORMANCE IN HIGH-TEMPERATURE HF ENVIRONMENTS

Material	Maximum Surface Temperature[1] (K)	Assumed Film Emissivity (ϵ)	Assumed Emissivity Correction[2] (K)	Max. Surface Temp. Including Assumed Emissivity Correction (K)	Remarks
$LaCrO_3$, HF-122	1365	0.4	85	1450	Withstood 2400K shock; LaF_3 film was 0.029 in thick; mp LaF_3 = 1766K, mp CrF_2 = 1373K; subl. CrF_3 = 1370K
LaB_6, HF-102	1636	0.4	120	1756	Withstood 3000K shock, LaF_3 film was 0.004 in thick
Si_3N_4 (MgO doped), HF-127	< 1135	-	-.	< 1135	Reacted at all observable temperatures, catastrophic reaction above 1450K
$La_2O_3 \cdot Si_3N_4$, HF-125	$\sim$ 1495	0.4	100	1595	Specimen cracked; also too porous
Sc, HF-119	1400	0.5	64	1464	mp ScF_3 = 1788K
TiAl, HF-124	1163	0.5	44	1207	
NiAl, HF-109	1375	0.5	61	1436	mp NiF_2 = 1430K
Ni-270, HF-110	1390	0.5	62	1452	
Y, HF-111	1365	0.5	59	1424	mp YF_3 = 1425K

[1] Remote optically observed surface temperature of emergence of rapid reaction (including window corrections of 15-23K and mirror if manual reading of 20K).

[2] From NBS Monograph 30.

The temperatures given in Table 3 were determined by observing the surface temperature at which the fluoride film ceases to be protective. In some cases, the "break point" could be seen on the pyrometer traces by a discontinuous rapid rise in temperature from the exothermic reaction as the material is no longer protected by a fluoride film. For rod specimens (HF-116 and HF-114), when such a "break point" occurred, very rapid reaction led to complete corrosion of the specimen so that the "after reaction" temperatures (noted by << in Table 3) could be recorded and, possibly, the last manual pyrometer reading before the very rapid reaction.

Perhaps the most difficult maximum surface temperatures to obtain are for subliming fluorides, since the "break point" is a gradual transition to ever-increasing rates of reaction, as with graphite and alumina. Therefore, all graphite data from previous report[1,2] has been plotted and is shown in Figure 2. The assumption is made that if the surface temperature was < 1000K, the surface temperature is equal to the base thermocouple temperature. The glassy carbon run (HF-13) is normalized for a 1.2-cm (0.5 in)-thick specimen. The data (excluding the zero-corrosion samples) are fit to a least-squares straight line which yields a maximum surface temperature of 1009K excluding emissivity, and for $\varepsilon = 0.9$, 1014K.

B. DISCUSSION OF TEST RESULTS FOR SPECIFIC CANDIDATES

1. Beryllia

Two grades of BeO were obtained——National Beryllia Corporation Berlox K-150 and high purity Y-12 material. From Table 1 it can be seen that the Y-12 grade contained < 400 wppm Li as its main impurity, whereas the Berlox material has $\sim$ 0.5% impurities apparently from a clay hot-pressing aid.

The data for maximum surface temperature with near-zero corrosion are based on the rapid rise in surface temperature above the points noted in Table 3. Figure 3 shows the temperature versus time data for Berlox. The data for the Y-12 material is shown in Figure 4. For Berlox, the film created an initially darker appearance on the top surface of the sample during the run as compared to the edges. This is attributed to the thicker film on top as compared to the edge. Because of this initial darker appearance, it was possible to note when the top and edges appear equally hot. The temperature where this occurred coincided with the point where surface temperature began to rapidly rise——or where film protection ceased. The darker-film phenomena did not occur for the Y-12 BeO so that it may be impurity-related. The Y-12 grade appeared to survive $\sim$ 65K higher surface temperatures before failure.
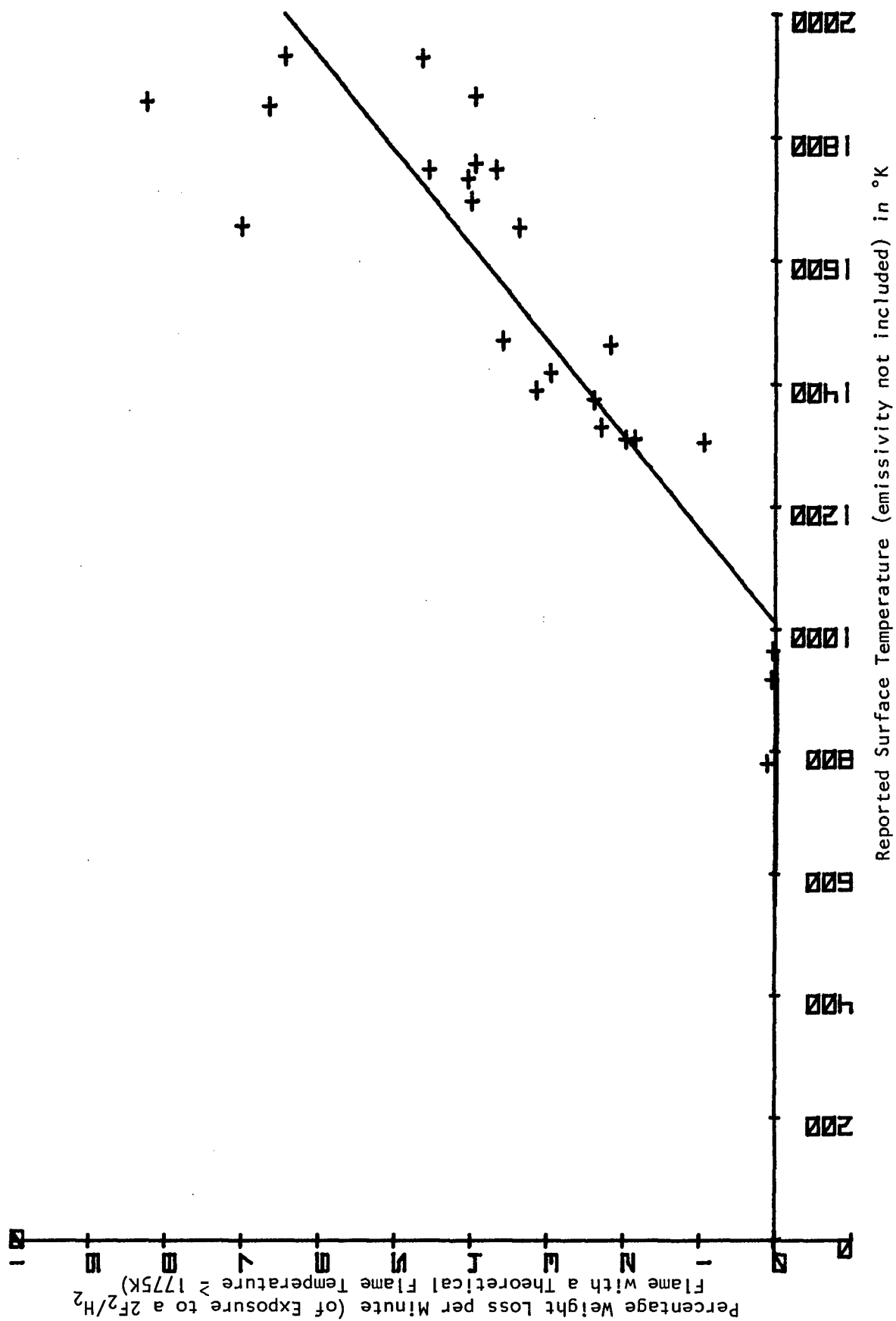
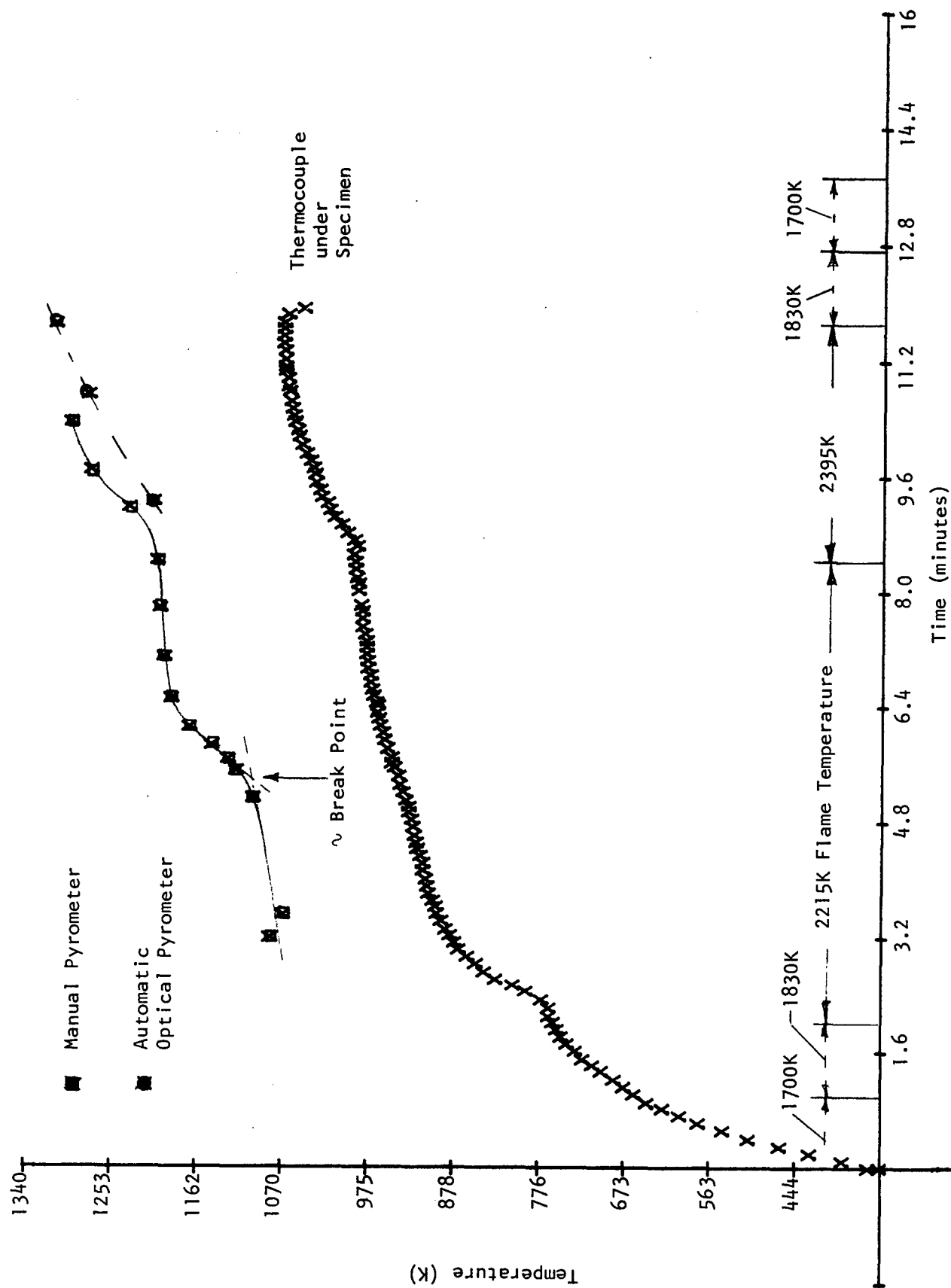Figure 2. CORROSION RATE DATA FOR CARBON.

Figure 3. TEMPERATURE VERSUS TIME CURVE FOR BERLOX K-150 (BERYLLIA) EXPOSED TO $2F_2/H_2$ (Run HF-133).
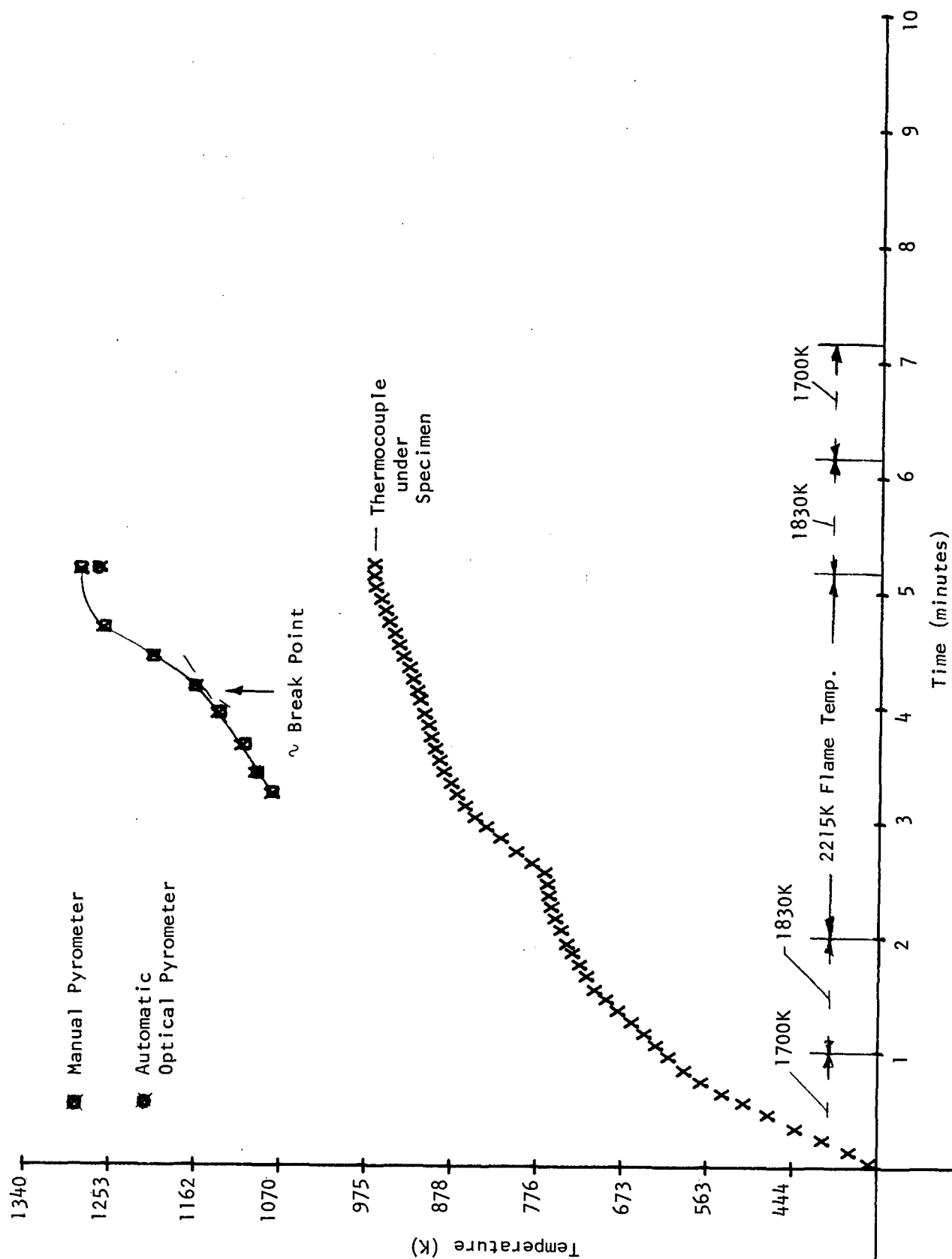
Figure 4. TEMPERATURE VERSUS TIME CURVE FOR Y-12 BERYLLIA EXPOSED TO $2F_2/H_2$ (Run HF-134).

The melting temperature of BeF_2 is from 825-1075K,[3,4] and an oxyfluoride $(2BeO \cdot 5BeF_2)$ may[4] or may not[5] exist——melting at 1025K.[4] Therefore, the maximum surface temperature for near-zero reaction (Table 3) of BeO is reasonable, especially since both the fluoride and oxyfluoride would be present as a glass with viscosity decreasing with increasing temperature past its melting range. That BeO reacts rapidly at 1273K with F_2 had also been established in an earlier General Electric Company study[6] of refractories in halogen environments.

2. Magnesia

Previous tests on magnesia (MgO) were aimed at determining the maximum flame temperature for near-zero corrosion. A surface temperature of 1158K was reported with a 2200K maximum flame temperature (HF-73). Reexamining Run HF-74 where MgO failed at a flame temperature of 2320K, a "break point" of 1248K was determined after which the temperature rapidly rises to 1560K (emissivity of 0.4, +100K included). This data is shown in Table 3 along with the Runs HF-137 (single crystal) and HF-116 (rod specimen). The single crystal run was almost identical to the polycrystalline MgO run. A "break point" occurred at 1241K after which a rapid temperature rise to 1464K (emissivity of 0.4, +84K included) occurred. Therefore, it appears that (1) there is little or no effect of grain boundaries for MgO; (2) fluoride film protection on MgO ceases at 150-175K below the eutectic (MgF_2-MgO) temperature of 1487K; and (3) the exothermic heat of reaction forming MgF_2 after film protection is lost is a large additional heat source causing the discontinuous rapid rise in temperature to or somewhat above the eutectic temperature. In fact, for the MgO single crystal, HF-137, the eutectic (MgF_2-MgO) caused a characteristic endothermic drop in the recorded temperature (automatic optical pyrometer). This cooling was observed visually for a few seconds. No flow (He, H_2, F_2) changes had occurred. The liquid surface layer was previously determined to be the eutectic oxide-fluoride mixture by X-ray diffraction of a melted droplet.

3. Alumina

Further tests on alumina (Al_2O_3) have involved the thermocouple experiments to further define the surface temperature. The temperature versus time data are shown in Figure 5 for surface temperatures less than that where film stability ceases, and in Figure 6 for temperatures above the maximum surface temperature for near-zero corrosion. As previously reported, the ΔT between top and bottom thermocouples was approximately zero for the first 30 seconds of heatup, until the specimen was above $\sim$ 600K. The ΔT then increases continuously reaching $\sim$ 200K maximum. The pyrometer readings and top thermocouples agree well below 1100K (where emissivity corrections are generally < 50K) and are only 50-100K different above 1100K. The Run HF-132 showed a "break point" in the top thermocouple scan, indicating the film failure point. Such a "break point" occurred with another run (HF-135) on the automatic pyrometer scan.
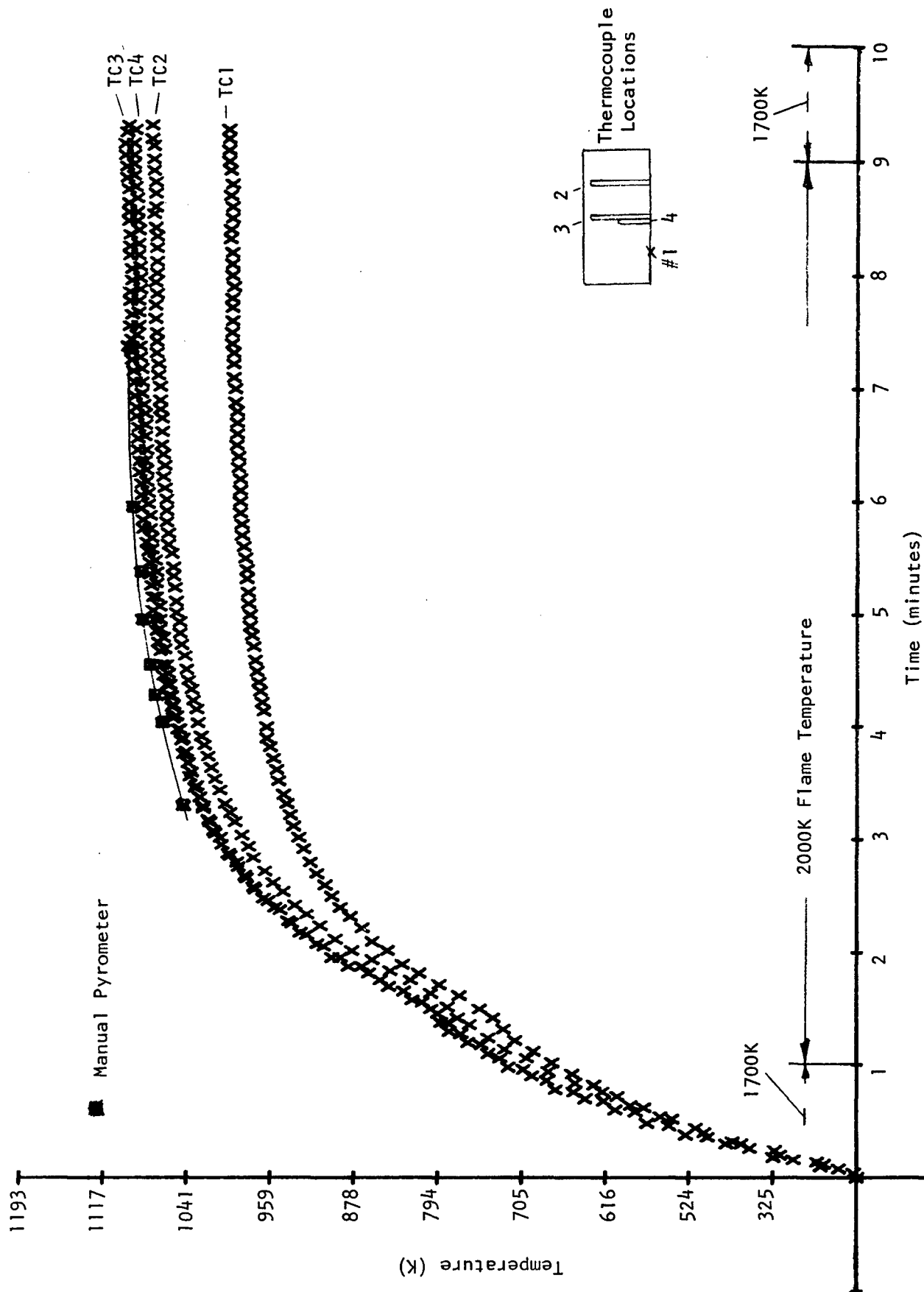
Figure 5. TEMPERATURE VERSUS TIME CURVES FOR THERMOCOUPLE EXPERIMENT WITH ALUMINA (RUN HF-131) BELOW MAXIMUM SURFACE TEMPERATURE FOR NEAR-ZERO CORROSION.
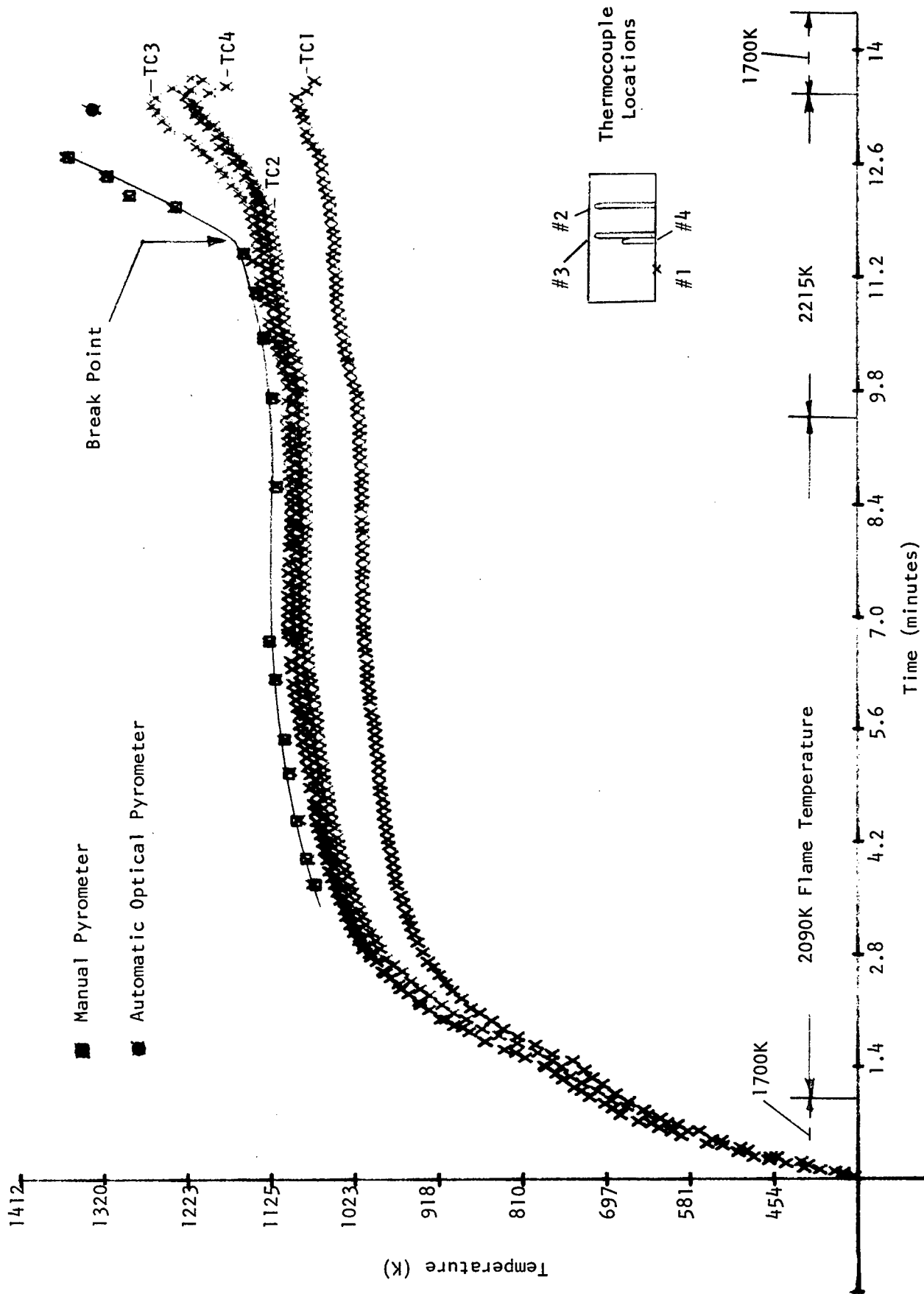
Figure 6. TEMPERATURE VERSUS TIME CURVES FOR THERMOCOUPLE EXPERIMENT WITH ALUMINA (RUN HF-132) WITH TEMPERATURE EXCEEDING THE MAXIMUM SURFACE TEMPERATURE FOR NEAR-ZERO CORROSION.

These "break points" were rarely seen with Al_2O_3 specimens—probably because the automatic pyrometer initiation point and the film failure points are so similar.

The single crystal (HF-121) of Al_2O_3 appeared to react like the polycrystalline material, except with a possibly higher corrosion rate. By X-ray diffraction, the index of the face of the sapphire single crystal which was exposed to the torch was the (010). Thus, this face may result in somewhat more favorable reaction kinetics.

The data from all alumina runs (excluding Run HF-22 with specimen off-centered and erratic gas flows and HF-24 with a cracked specimen and lost process He) are shown in Figure 7. Sapphire runs are circled. Data from two cracked specimens(*) are shown to indicate the accelerated rate of reaction if cracking occurs. Below 1100K, the surface temperature was estimated from base thermocouple data and data from Run HF-90. From this curve, the maximum zero-corrosion temperature appears to be $\sim$ 1110K; or with emissivity corrections for $\varepsilon = 0.4$, $\sim$ 1165K.

4. Lanthanum Hexaboride

As mentioned previously,[2] lanthanum hexaboride (LaB_6) forms a white adherent fluoride film immediately on initial exposure to a fluorine/ hydrogen environment. The white film is a strong contrast to the bluish purple LaB_6 and by scanning electron microscopy was shown[2] to be $\sim$ 100 μm (0.004 in) thick after 34 minutes of exposure to $2F_2/H_2$ flame temperatures > 1700K. Further testing of LaB_6 involved increasing flame temperatures above 2400K to 3000K in $\sim$ 100K increments (Runs HF-96 to HF-103). After ten runs on a single sample with a total of 87 minutes at flame temperature > 1700K, the cumulative weight loss was less than 0.6% with virtually no detectable dimensional changes. In fact, weight losses tended to decrease somewhat as the flame temperatures increased. The LaF_3 coatings appeared to sinter or densify with high temperature exposure for prolonged periods. The LaF_3 layer may also become more protective and thinner as the surface temperature increases.

After 10.75 minutes of 3000K, $2F_2/H_2$ flame temperature (HF-102), with no observable corrosion, the temperature was further increased by decreasing the fluorine flow to $1.2F_2/H_2$. At this point, some film flowing was visually observable, yet no dramatic temperature increase characteristic of surface exothermic reaction, when protection from a fluoride film ceases, occurred. The LaF_3 film appeared viscous and protective. Observable flowing of the LaF_3 film occurred in a temperature range of 1616-1636K (uncorrected for emissivity). Adding 120K for $\varepsilon = 0.4$, the maximum use range is 1736-1756K. Even after "failure", the sample retained its configuration and catastrophic corrosion did not occur.
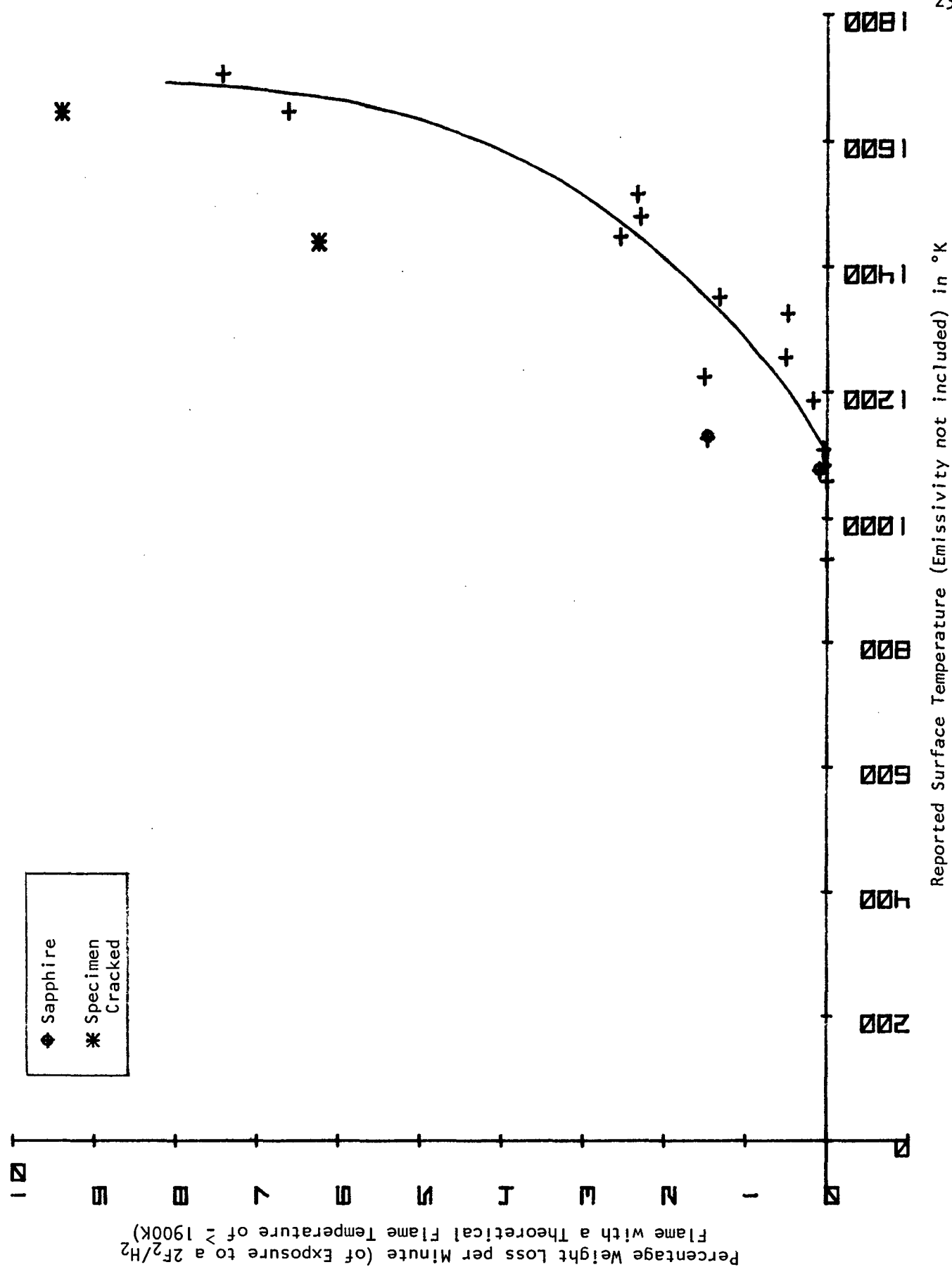
Figure 7. CORROSION RATE DATA FOR ALUMINA.

Reported Surface Temperature (Emissivity not included) in °K

Percentage Weight Loss per Minute (of Exposure to a $2F_2/H_2$ Flame with a Theoretical Flame Temperature of $\geq$ 1900K)

Legend:
● Sapphire
✻ Specimen Cracked

23

A further experiment (HF-103) demonstrated the thermal shock resistance of the material. Direct heating of LaB_6 in a 3000K flame and subsequent rapid cooling after equilibration by instantaneously securing the flame showed no indication of thermal shock cracking. Conventional non-metallic specimens require the programmed heating cycle to avoid frag-mentation. Other than graphite, LaB_6 and $LaCrO_3$ (mentioned previously) are the only nonmetallic specimens that have withstood direct heating with a flame temperature > 2000K. [Note: BeO was not tested by direct heating and would possibily have survived this thermal shock without cracking.]

Figure 8 shows the LaB_6 sample after all the $2F_2/H_2$ torch tests. The shape retention is readily seen. A closeup of the sample is shown in Figure 9, where the LaF_3 film and the "teardrops" of clear, melted LaF_3 are very noticeable. The flame velocity caused sufficient surface film flowing to create these small drops, yet very little change in the top surface of the specimen occurred.

To summarize, these experiments indicate that LaB_6 can withstand surface temperatures of 1736K to 1756K with near-zero corrosion. Previously, the vaporization of LaF_3 was demonstrated to be low——below 1640K. No corrosion would be expected below that temperature. The excellent behavior of LaB_6 probably results from the adherent, relatively dense LaF_3 coating which may have a microcracking stress relief mechanism.[2] The dense coating probably results from the relatively high atomic density (atoms/cc) of LaB_6. Even after melting, the LaF_3 film remains intact minimizing reaction of the LaB_6 substrate. The excellent thermal shock resistance and machining possibilities (with electronic techniques because of its electrical conductivity) are additional factors favoring this material as a nozzle candidate.

5. Metallics

Because of their high thermal conductivities, it was difficult to heat metallic materials to a sufficiently high temperature to induce failure.[2] However, by using the higher flame temperature (2400-3000K), as with LaB_6, it was possible to achieve surface temperatures sufficiently high for breakdown of their fluoride films. This point was followed in all cases by catastrophic failure resulting from the heat input from the exothermic, uninhibited fluoride reaction plus the heat being trans-mitted by the flame.

Considering Table 3, TiAl reacted at virtually the same temperature as Al_2O_3, which is reasonable since AlF_3 is the protective layer for both. However, NiAl reacted at the NiF_2 melting point which is over 200K higher than the AlF_3 film failure temperature. The only apparent advantage of NiAl over pure Ni is that NiAl melts at 1920K compared to a Ni melting point of 1725K. Yttrium also reacted catastrophically when the melting point of YF_3 was exceeded by shattering completely into pieces as it reacted.
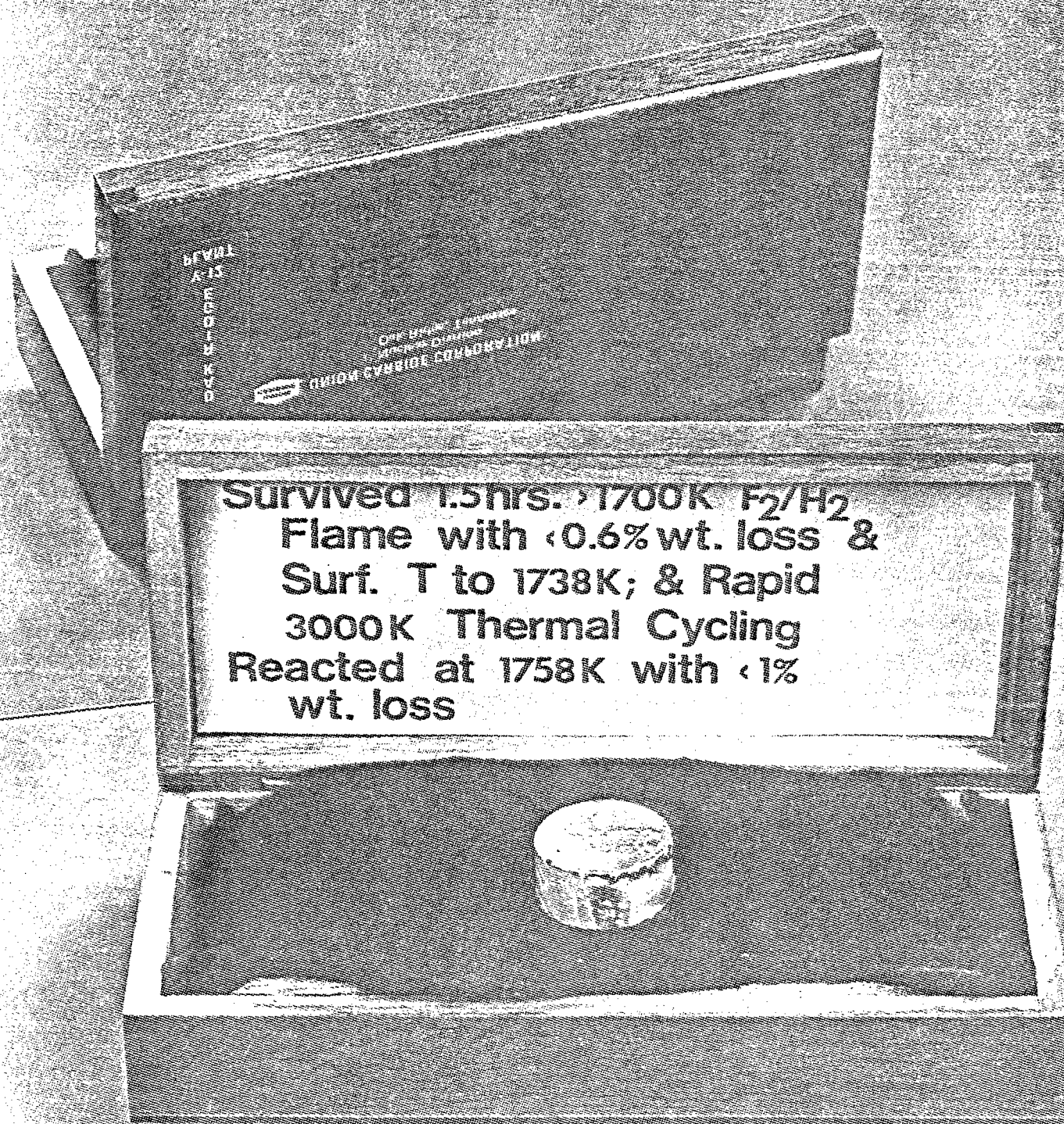
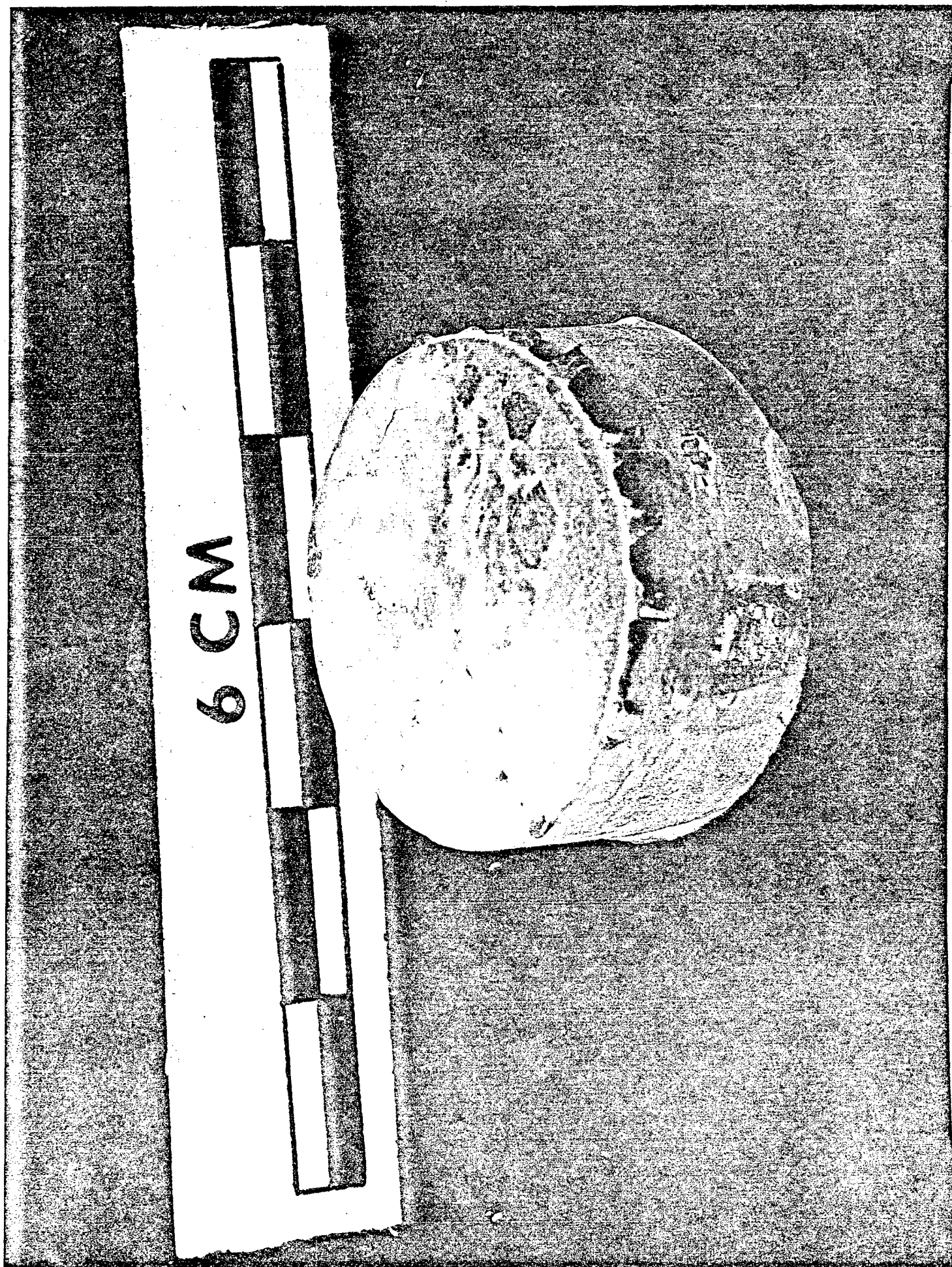Figure 8.   LANTHANUM HEXABORIDE SAMPLE AFTER HIGH-TEMPERATURE $2F_2/H_2$ TESTS.

Figure 9. LANTHANUM HEXABORIDE SAMPLE—CLOSEUP SHOWING MELTED LaF_3 SURFACE AND "TEARDROPS".

Melted droplets from NiAl, Ni, and Sc were analyzed by X-ray diffraction from samples near the center of the droplets. Only the respective metals were detected. Thus, the Sc data are somewhat anomalous. It appears that ScF_3 ceases to be protective (spalls off, cracks, or otherwise fails) approximately 300K below its reported melting point. When failure occurs, as with all the metallics, a large jump in surface temperature occurs, resulting in melting of the metal substrate.

While the maximum surface temperature from near-zero corrosion of the metallic specimens (excluding TiAl) are relatively high, these temperatures represent 75-85% of the substrate melting points (Tm). Significant loss of high-temperature strength and configurational stability would be expected when diffusional creep occurs (over 0.7 Tm in °K). Also, if film failure occurs, the resulting rapid deterioration of the part would be unacceptable.

6. SILICON NITRIDE AND LANTHANUM-SILICON OXYNITRIDE

Silicon nitride, Si_3N_4, (with $\sim$ 5% MgO additive) was the only nonfluoride-film former listed in Table 3. That sample, HF-127, reacted at all observable temperatures, becoming catastrophic above 1450K where no protection from the MgO dopant would occur. Weight loss was excessive, 29.3% after 4 minutes of 2215 K flame temperature. Its behavior may be compared to SiC, another nonfilm former, which lost 27 weight % after 4.5 minutes at 2000 K flame temperature. The Si_3N_4 sample had a thin, friable, lace-like coating after the run. This was identified by X-ray diffraction as MgF_2.

Because of the low thermal expansion and good mechanical properties, silicon nitride is considered to be a high toughness ceramic and is under study for turbine blade applications. For rigorous thermal changes it would appear to be a good candidate material. For a $2F_2/H_2$ environment, however, it reacts rapidly—presumably forming NF_3 (or N_2) and SiF_4. These species are noneutectic-forming, volatile fluorides. Thus, an increased dopant level with a fluoride-film former could yield a very promising material with the good properties of Si_3N_4 while forming a protective fluoride layer. For this reason, the compound $La_2O_3 \cdot Si_3N_4$[7] was prepared by reactive hot pressing a 1:1 molar mixture of calcined La_2O_3 and Si_3N_4 at 1600°C at 21 MPa ($\sim$ 3 ksi) for 1 hour. From Table 2, it can be seen that the oxynitride was only 80% dense. On testing in $2F_2/H_2$, the specimen developed cracks even with programmed heating. Nevertheless, the maximum surface temperature for near-zero reaction appears quite high (Table 3). Because of the porosity, the specimen appeared to be reacted throughout to some extent but was protected well from complete destruction, considering its high porosity. The upper use-temperature seems to be $\sim$ 150K less than for LaB_6, but the apparent coating failure could have been influenced by the surface cracking and specimen porosity. It should be noted that $La_2O_3 \cdot Si_3N_4$ is apparently not very reactive with water, since no weight change resulted on immersion of a sample in water for 1 week.

The cracking failure of $La_2O_3 \cdot Si_3N_4$ may be caused by either a high thermal expansion coefficient or by buildup of SiF_4 vapor in the pores followed by pore blockage. A more dense specimen should be examined to resolve the cause of the cracking. Additionally, the compound $La_2O_3 \cdot 2Si_3N_4$ has been reported[7] and could exhibit good behavior in the $2F_2/H_2$ environment. Further testing along these lines including doping silicon nitride is in progress.

CONCLUSIONS

The continuation of materials testing with 36 runs in the HF facility has revealed the following:

1. Surface temperatures of emergence of rapid reaction depend upon the failure of the protective fluoride film to limit substrate exposure or to kinetically inhibit the fluoriding reaction.

2. Fluoride-film failure can occur by melting, sublimation, vaporization, spalling, or microcracking. For most materials, film failure occurs at melting or sublimation. Magnesia (MgO) and Sc form fluorides which fail to protect the substrate 150-300K below their respective fluoride melting points.

3. In general, when corrosion occurs, materials with subliming fluorides (i.e., Al_2O_3, C) have lower rates of corrosion after failure and have better configurational stability than materials with melting fluorides. For LaB_6, the fluoride film is sufficiently viscous to protect to some extent after film melting to retain sample configuration.

4. Immediately after failure of the fluoride film, the observed surface temperature rises from the large extra heat input from the exothermic fluoriding reaction in addition to the heat input from the flame.

5. There is little apparent effect of grain boundaries from single and polycrystalline Al_2O_3 and MgO runs or purity (at a nominal 99% level) on the upper use-temperature.

6. The best performers in the $2F_2/H_2$ torch on the basis of maximum surface temperature for near-zero corrosion:

   LaB_6 [1750K] > $La_2O_3 \cdot Si_3N_4$ [1600K] > (Sc, $LaCrO_3$, Ni, NiAl, Y)
   [1450] > MgO [1300K] > (BeO, Al_2O_3, TiAl) [1200K] > C [1000K].

REFERENCES

1. G. W. Weber, L. Kovach, C. E. Holcombe, and J. B. Condon, "Evaluation of Materials for Use in Hydrogen-Fluorine Environments," Report Y/DA-7321, Union Carbide Corporation, Nuclear Division, Oak Ridge Y-12 Plant, Oak Ridge, Tennessee; June 17, 1977.

2. C. E. Holcombe, L. Kovach, and G. W. Weber, "Materials for High-Temperature Hydrogen-Fluorine Environments," Report Y/DA-7477, Union Carbide Corporation, Nuclear Division, Oak Ridge Y-12 Plant, Oak Ridge, Tennessee; October 3, 1977.

3. JANAF Thermochemical Tables, 2nd Edition; D. R. Stull and H. Prophet, Project Directors; National Bureau of Standards, Washington, D. C.; 1971.

4. K. Illig, M. Hosenfeld, and H. Fischer, In Beryllium, Its Production and Application, R. Rimbach and A. J. Michel, Translators, The Chemical Catalog Company, Inc., New York, 1932, pp 39-51.

5. Carlos E. Bamberger, 1977, Personal Communication of 1968 Data, Oak Ridge National Laboratory, Oak Ridge, Tennessee.

6. "High-Flux Reactor Materials Gaseous Fuels Research", Report GEMP-334B, General Electric Company, pp 161-184.

7. R. R. Wills, R. W. Stewart, J. A. Cunningham, and J. M. Wimmer, "The Silicon Lanthanide Oxynitrides", J. Matls Sci., 11, 749-59 (1976).

APPENDICES

APPENDIX I. SUMMARY OF TEST CONDITIONS DURING THE EXPOSURE OF SPECIMENS TO A HYDROGEN-FLUORINE FLAME

Run No.	HF-93	HF-96	HF-97	HF-98
Specimen Identification	Sc_2O_3	LaB_6	LaB_6	LaB_6
Source		HF-78	HF-96	HF-97
Nozzle Flows, scfm				
Helium	3.8 3.6 3.6	3.8 3.6 3.0 3.6 3.8	3.8 3.6 2.85 3.6 3.8	3.8 3.6 2.7 3.6 3.8
Fluorine	0.9 1.0 1.2	0.9 1.0 1.6 1.0 0.9	0.9 1.0 1.7 1.0 0.9	0.9 1.0 1.73 1.0 0.9
Hydrogen	0.45 0.5 0.6	0.45 0.5 0.8 0.5 0.45	0.45 0.5 0.85 0.5 0.45	0.45 0.5 0.865 0.5 0.45
(total)	5.15 5.1 5.4	5.15 5.1 5.4 5.1 5.15	5.15 5.1 5.40 5.1 5.15	5.15 5.1 5.295 5.1 5.15
Theoretical Flame Temperature, K	1700 1830 2000	1700 1830 2400 1830 1700	1700 1830 2450 1830 1700	1700 1830 2535 1830 1700
Duration of Run, min	1 1 1.25	1 1 4.67 1 1	1 1 4.75 1 1	1 1 4.75 1 1
Optical Pyrometer, °C(a)	No indication < 850	1038	1060	1125
Thermocouple Reading under the Specimen, °C	743	815	848	842

(a) Direct uncorrected readings

Run No.	HF-99					HF-100					HF-101				
Specimen Identification	LaB$_6$					LaB$_6$					LaB$_6$				
Source	HF-98					HF-99					HF-100				
Nozzle Flows, scfm															
Helium	3.8	3.6	2.55	3.6	3.8	3.8	3.6	2.45	3.6	3.8	3.8	3.6	2.3	3.6	3.8
Fluorine	0.9	1.0	1.8	1.0	0.9	0.9	1.0	1.9	1.0	0.9	0.9	1.0	1.95	1.0	0.9
Hydrogen	0.45	0.5	0.9	0.5	0.9	0.45	0.5	0.95	0.5	0.9	0.45	0.5	0.976	0.5	0.9
	5.15	5.1	5.25	5.1	5.15	5.15	5.1	5.30	5.1	5.15	5.15	5.1	5.226	5.1	5.15
Theoretical Flame Temperature, K	1700	1830	2615	1830	1700	1700	1830	2690	1830	1700	1700	1830	2770	1830	1700
Duration of Run, min.	1	1	4.75	1	1	1	1	5	1	1	1	1	4.83	1	1
Optical Pyrometer, °C			1120					1170					1193		
Thermocouple Reading under the Specimen, °C			838					843					903		

Run No.	HF-102				HF-103	HF-108			HF-109		HF-110				
Specimen Identification	LaB$_6$				LaB$_6$	NiAl			NiAl		Ni-270				
Source	HF-101				HF-102	HF-29			HF-108		HF-43				
Nozzle Flows, scfm															
Helium	3.8	3.6	2.15	2.15(b)	2.15	3.8	3.6	3.3	3.0	2.7	3.0	2.7	2.55	2.45	2.15
Fluorine	0.9	1.0	2.0	1.0	2.0	0.9	1.0	1.4	1.6	1.73	1.6	1.73	1.8	1.9	2.0
Hydrogen	0.45	0.5	1.0		1.0	0.45	0.5	0.7	0.8	0.87	0.8	0.865	0.9	0.95	1.0
	5.15	5.1	5.15		5.15	5.15	5.1	5.4	5.4	5.30	5.4	5.3	5.25	5.30	5.15
Theoretical Flame Temperature, K	1700	1830	2840	2840+	2840	1700	1830	2215	2400	2535	2400	2535	2615	2690	2840
Duration of Run, min	1	10.75	3.42		3.75	1	1	4.77	5.33	4.52	4.25	5.25	3.0	2.0	1.5
Optical Pyrometer, °C			1375		925			830 Manual		1295	825 Manual	985	1010-1040	1035	1250
Thermocouple Reading under the Specimen, °C			1080		842			700		1065	700	800	895	895	1200

(b)F$_2$ flow was reduced in stages to 1.4, 1.25, and 1.0 scfm when flame-out occurred.

Run No.	HF-111		HF-112(c)				HF-113(c)					HF-114(c)					
Specimen Identification	Yttrium		Al₂O₃ – HF-84				Al₂O₃					Al₂O₃					
Source			TRW A10206				TRW A10205					HF-113					
Nozzle Flows, scfm																	
Helium	3.0	2.7	3.8	3.6	3.3	3.0	3.8	3.6	3.6	3.6	3.8	3.8	3.6	3.4	3.3	3.6	3.8
Fluorine	1.6	1.73	0.9	1.0	1.4	1.6	0.9	1.0	1.2	1.0	0.9	0.9	1.0	1.3	1.4	1.0	0.9
Hydrogen	0.8	0.865	0.45	0.5	0.7	0.8	0.45	0.5	0.6	0.5	0.45	0.45	0.5	0.65	0.7	0.5	0.45
	5.4	5.3	5.15	5.1	5.4	5.4	5.15	5.1	5.4	5.1	5.15	5.15	5.1	5.35	5.4	5.1	5.15
Theoretical Flame Temperature, K	2400	2535	1700	1830	2215	2400	1700	1830	2000	1830	1700	1700	1830	2120	2215	1830	1700
Duration of Run, min	2.75	1.12	1	1	4.08	0.08	1	1	4.5	1	1	1	1	4	2.25	1	1
Optical Pyrometer, °C	965	1280	1280				< 750 Manual					1155					
Thermocouple Reading under the Specimen, °C	1090		863				748					NA					

(c) Specimen was previously exposed to the HF flame for periods of 8.5 and 13 minutes; the flame was not operating properly, however, and the runs were not considered valid.

Run No.	HF-115[d]	HF-116[d]	HF-118	HF-119
Specimen Identification	MgO	MgO	Scandium	Scandium
Source	TRW	TRW HF-115	Research Chem. Lot. Sc-M-3-272D	HF-118
Nozzle Flows, scfm				
Helium	3.8 3.6 3.3 3.0	3.8 3.6 2.6 2.45	3.0 2.6	2.45
Fluorine	0.9 1.0 1.4 1.6	0.9 1.0 1.7 1.9	1.6 1.7	1.9
Hydrogen	0.45 0.5 0.7 0.8	0.45 0.5 0.85 0.95	0.8 0.85	0.95
	5.15 5.1 5.4 5.4	5.15 5.1 5.15 5.30	5.4 5.15	5.30
Theoretical Flame Temperature, K	1700 1830 2215 2395	1700 1830 2550 2690	2400 2550	2690
Duration of Run, min	1 1 3.5 4.5	1 1 3.33 1.92	3.3 2.78	0.77
Optical Pyrometer, °C	No Indication < 850	No Indication Manual > 1100[e]	1047	1280
Thermocouple Reading under the Specimen, °C	None	None	675	580

[d] MgO powder used at specimen support points
[e] Temperature rose rapidly near end of run

Run No.	HF-120				HF-121					HF-122						
Specimen Identification	Sapphire – Single Crystal				Sapphire – Single Crystal					LaCrO$_3$						
Source	ESPI				HF-120											
Nozzle Flows, scfm																
Helium	3.8	3.6	3.6	3.8	3.8	3.6	3.45	3.6	3.8	3.8	3.6	3.3	3.1	3.0	3.6	3.8
Fluorine	0.9	1.0	1.2	0.9	0.9	1.0	1.3	1.0	0.9	0.9	1.0	1.4	1.5	1.6	1.0	0.9
Hydrogen	0.45	0.5	0.6	0.45	0.45	0.5	0.65	0.5	0.45	0.45	0.5	0.7	0.75	0.8	0.5	0.45
(total)	5.15	5.1	5.4	5.15	5.15	5.1	5.40	5.1	5.15	5.15	5.1	5.4	5.35	5.4	5.1	5.15
Theoretical Flame Temperature, K	1700	1830	2000	1700	1700	1830	2105	1830	1700	1700	1830	2215	2320	2395	1830	1700
Duration of Run, min	1	1	5	1	1	1	5	1	1	1	1	3.83	1.67	4.17	0.83	1
Thermocouple Reading under the Specimen, °C	657				678					740						
Optical Pyrometer, °C(a)	No Indication Manual pyrometer – no indication				No Indication Manual – 818°C					1065						

(a) Manual pyrometer – no indication

Run No.	HF-123	HF-124	HF-125					HF-126						
Specimen Identification	LaCrO$_3$	TiAl	La$_2$O$_3$·Si$_3$N$_4$					Al$_2$O$_3$						
Source	HF-122	AFML						Coors						
Nozzle Flows, scfm														
Helium	3.0	3.3	3.8	3.6	3.3	3.6	3.8	3.8	3.3	3.3	3.0	3.3	3.3	3.8
Fluorine	1.6	1.4	0.9	1.0	1.4	1.0	0.9	0.9	1.0	1.3	1.4	1.3	1.0	0.9
Hydrogen	0.8	0.7	0.45	0.5	0.7	0.5	0.45	0.45	0.5	0.65	0.7	0.65	0.5	0.45
	5.4	5.4	5.15	5.1	5.4	5.1	5.15	5.15	4.8	5.25	5.1	5.25	4.8	5.15
Theoretical Flame Temperature, K	2395	2215	1700	1830	2215	1830	1700	1700	1910	2150	2280	2150	1910	1700
Duration of Run, min	2.33	3.93	1.0	1.0	4.0	1.0	0.883	1.0	0.58	0.58	2.08	0.67	0.58	1.0
Thermocouple Reading under the Specimen, °C	700	813			747						680			
Optical Pyrometer, °C	1048	1435			1360						965			

Run No.	HF-127					HF-128							HF-129(a)
Specimen Identification	Si₃N₄ (MgO doped 5%)					Al₂O₃							ATJ Graphite
Source						Coors							
Nozzle Flows, scfm													
Helium	3.8	3.6	3.3	3.6	3.8	3.8	3.3	3.3	3.0	3.3	3.3	3.8	3.0
Fluorine	0.9	0.1	1.4	1.0	0.9	0.9	1.0	1.3	1.4	1.3	1.0	0.9	1.4
Hydrogen	0.45	0.5	0.7	0.5	0.45	0.45	0.5	0.65	0.7	0.65	0.5	0.45	0.7
	5.15	5.1	5.4	5.1	5.15	5.15	4.8	5.25	5.1	5.25	4.8	5.15	5.1
Theoretical Flame Temperature, K	1700	1830	2215	1830	1700	1700	1910	2150	2280	2150	1910	1700	2280
Duration of Run, min	1.0	1.0	4.0	1.0	1.0	1.0	0.58	0.58	2.67	0.58	0.58	1	4.13
Thermocouple Reading under Specimen, °C			780						735				750
Optical Pyrometer, °C			1335						1220				1280

(a) To check flame alignment

Run No.	HF-130	HF-131	HF-132	HF-133
Specimen Identification	Al$_2$O$_3$	Al$_2$O$_3$	Al$_2$O$_3$	BeO
Source	Coors	HF-130	HF-131	National Beryllia, Berlox K-150
Nozzle Flows, scfm				
Helium	3.8 3.7 3.8	3.8 3.6 3.8	3.8 3.5 3.3 3.8	3.8 3.6 3.3 3.0 3.6 3.8
Fluorine	0.9 1.1 0.9	0.9 1.2 0.9	0.9 1.3 1.4 0.9	0.9 1.0 1.4 1.6 1.0 0.9
Hydrogen	0.45 0.55 0.45	0.45 0.6 0.45	0.45 0.65 0.7 0.45	0.45 0.5 0.7 0.8 0.5 0.45
	5.15 5.35 5.15	5.15 5.4 5.15	5.15 5.45 5.4 5.15	5.15 5.1 5.4 5.4 5.1 5.15
Theoretical Flame Temperature, K	1700 1900 1700	1700 2000 1700	1700 2090 2215 1700	1700 1830 2215 2395 1830 1700
Duration of Run, min	1.0 7.25 1.0	1.0 8.0 1.0	1.0 8.33 3.92 1.0	1.0 1.0 6.33 3.33 1.0 1.0
Thermocouple Readings under the Specimen, °C	—	—	—	805
Optical Pyrometer, °C	No indication Manual pyrometer 740°C after 5 min	No indication Manual pyrometer 820°C after 7 min 20 sec	1035	1025
Thermocouple Experiment Readings, °C				
#1	687	726	810	
#2	758	798	931	
#3	775	822	981	
#4	768	815	927	

HF-134

Run No.	HF-134			
Specimen Identification	BeO			
Source	Y-12			
Nozzle Flows, scfm				
Helium	3.8	3.6	3.3	3.8
Fluorine	0.9	1.0	1.4	0.9
Hydrogen	0.45	0.5	0.7	0.45
	5.15	5.1	5.4	5.15
Theoretical Flame Temperature, K	1700	1830	2215	1700
Duration of Run, min	1.0	1.0	3.17	1.0
Thermocouple Reading under the Specimen, °C	700			
Optical Pyrometer, °C	978			

HF-135

Run No.	HF-135						
Specimen Identification	Al_2O_3						
Nozzle Flows, scfm							
Helium	3.8	3.3	3.3	3.0	3.3	3.3	3.8
Fluorine	0.9	1.0	1.3	1.4	1.3	1.0	0.9
Hydrogen	0.45	0.5	0.65	0.7	0.65	0.5	0.45
	5.15	4.8	5.25	5.1	5.25	4.8	5.15
Theoretical Flame Temperature, K	1700	1910	2150	2280	2150	1910	1700
Duration of Run, min	1.0	0.58	0.58	4.58	0.58	0.58	1.0
Thermocouple Reading under the Specimen, °C	650						
Optical Pyrometer, °C	1155						

HF-137

Run No.	HF-137				
Specimen Identification	Single Crystal MgO[c]				
Source	Materials Research				
Nozzle Flows, scfm					
Helium	3.8	3.6	2.85	3.6	3.8
Fluorine	0.9	1.0	1.7	1.0	0.9
Hydrogen	0.45	0.5	0.85	0.5	0.45
	5.15	5.1	5.4	5.1	5.15
Theoretical Flame Temperature, K	1700	1830	2450	1830	1700
Duration of Run, min	1.0	1.0	2.5	1.0	1.0
Thermocouple Reading under the Specimen, °C	735				
Optical Pyrometer, °C	1395				

[c] Specimen was previously exposed to the HF flame for periods of 8.5 and 13 mins; the flame was not operating properly, however, and the runs were not considered valid.

APPENDIX II. OBSERVATIONS ON TEST SPECIMENS EXPOSED TO A HYDROGEN-FLUORINE FLAME

Run No.	Material	Theoretical Flame Temperature (K)	Duration of Run (min)	Sample Surface Temperature(1) (K)	Weight Loss (%)	Diameter Loss (%)	Height Loss (%)	Measured Loss in Height (mm)	Remarks
HF-93	Sc₂O₃	1700 1830 2000	1 1 1.25	No indication < 1138					Specimen appeared to be cracked after 1 minute; broke apart after approximately 2 1/2 minutes
HF-96	LaB₆ HF-78	1700 1830 2400 1830 1700	1 1 4.67 1 1	1328	0.07	0	0	0	Brownish area on top lessened
HF-97	LaB₆ HF-96	1700 1830 2450 1830 1700	1 1 4.75 1 1	1350	0.04	0	0	0	Brownish area still visible
HF-98	LaB₆ HF-97	1700 1830 2535 1830 1700	1 1 4.75 1 1	1416	0.06	0	0	0	Brownish area still visible
HF-99	LaB₆ HF-98	1700 1830 2615 1830 1700	1 1 4.75 1 1	1410	0.05	0	0	0	Brownish area still visible

(1) Includes sight-port window correction only and represents the temperature observed during the hot-test portion of the run; for manual pyrometer observations; 20K degrees are also added for a mirror correction.

Run No.	Material	Theoretical Flame Temperature (K)	Duration of Run (min)	Sample Surface Temperature (K)	Weight Loss (%)	Diameter Loss (%)	Height Loss (%)	Measured Loss in Height (mm)	Remarks
HF-100	LaB6 HF-99	1700 1830 2690 1830 1700	1 1 5 1 1	1463	0.02	0	0.4	0.05	Brownish area faint
HF-101	LaB6 HF-100	1700 1830 2770 1830 1700	1 1 4.83 1 1	1486	0.02	0	0.4	0.05	Brownish area increased
HF-102	LaB6 HF-101	1700 1830 2840 2840+	1 1 10.75 3.42	1672	0.96	0.2	+1.8/-1.6	+0.23/-0.20	Partial melting of the fluoride layer took place. Specimen had a glazed appearance
HF-103	LaB6 HF-102	2840	3.75	1213	0.06	0	0.2	0.03	Coating on specimen turned from gray to white after exposure to room air
HF-108	NiAl HF-27	1700 1830 2215	1 1 4.77	Manual 1138	0.13	0	0	0	No change
HF-109	NiAl HF-108	2400 2535	5.33 4.52	1591	34.3	4.1	29.8	4.1	Melting and corrosion of a specimen took place. Melting on specimen surface per manual pyrometer, appeared at 1468K.
HF-110	Ni-270 HF-43	2400 2535 2615 2690 2840	4.25 5.25 3.0 2.0 1.5	1544	-	-	-	-	Specimen corroded and fused to Ni specimen support. Reaction at top surface started at 1390K

Run No.	Material	Theoretical Flame Temperature (K)	Duration of Run (min)	Sample Surface Temperature (K)	Weight Loss (%)	Diameter Loss (%)	Height Loss (%)	Measured Loss in Height (mm)	Remarks
HF-111	Yttrium	2400 2535	2.75 1.12	1576	-	-	-	-	Specimen melted. Melting and film burnoff started at 1365K
HF-112	Al₂O₃ (TRW) HF-84	1700 1830 2215 2400	1 1 4.08 1.08	1576	-	-	-	-	Specimen corroded; one small section left. Extensive corrosion noticed at 1478K
HF-113	Al₂O₃ (TRW) A-10205	1700 1830 2000 1830 1700	1 1 4.5 1 1	Manual < 1058	0.45	Length 0	0.39 & 0.62	0.03 & 0.03	Little change
HF-114	Al₂O₃ HF-113	1700 1830 2120 2215 1830 1700	1 1 4 2.25 1 1	1447	39.7	Length 0	26.0 & 51.6	1.7 & 2.1	Specimen corroded and thinned down
HF-115	MgO (TRW)	1700 1830 2215 2395	1 1 3.5 4.5	< 1138	0.16	Length 0	0.4 & 0	0.03 & 0	Top edge slightly rounded
HF-116	MgO (TRW)	1700 1830 2550 2690	1 1 3.3 1.92	Manual > 1410	-	-	-	-	Specimen corroded

Run No.	Material	Theoretical Flame Temperature (K)	Duration of Run (min)	Sample Surface Temperature (K)	Weight Loss (%)	Diameter Loss (%)	Height Loss (%)	Measured Loss in Height (mm)	Remarks
HF-118	Scandium	2400 2550	3.33 2.78	1336	+4.4	+2.1	+10.8	1.4	White coating on side of specimen
HF-119	Scandium HF-118	2690	0.77	1576	-	-	-	-	Specimen melted Started to go at 1395K
HF-120	Sapphire Single Crystal	1700 1830 2000 1830 1700	1 1 5 1 1	No indication " < 1138	0.5	0.5	0.6	0.08	Specimen appeared to be etched all over
HF-121	Sapphire HF-120	1700 1830 2105 1830 1700	1 1 5 1 1	Manual 1126	7.4	0.4 (average)	5.4 (average)	0.69 (average)	Specimen had cracks in it, but did not fall apart
HF-122	LaCrO$_3$	1700 1830 2215 2320 2395 1830 1700	1 1 3.83 1.67 4.17 0.83 1.0	1340	1.4	+2.0	+3.4	+0.43	Specimen had white coating all over except for small area on the bottom; almost one-half of top surface had a glaze and showed evidence of melting
HF-123	LaCrO$_3$ HF-122	2395	2.33	1338	0.3	0	0	0	Some cracking evident in the coating layer; condition of basic structure not visible.
HF-124	TiAl (AFML)	2215	3.93	1732	10.0	1.5	3.9	0.61	Specimen had a black nonadherent coating
HF-127	Si$_3$N$_4$ MgO doped	1700 1830 2215 1830 1700	1.0 1.0 4.0 1.0 1.0	1631	39.3	6.1-6.6	13.9	1.75	Specimen corroded and was covered with a white flaky coating

Run No.	Material	Theoretical Flame Temperature (K)	Duration of Run (min)	Sample Surface Temperature (K)	Weight Loss (%)	Diameter Loss (%)	Height Loss (%)	Measured Loss in Height (mm)	Remarks
HF-125	$La_2O_3 \cdot Si_3N_4$	1700 1830 2215 1830 1700	1 1 4 1 0.883	1656	13.5	+0.4	+0.4	0.05	Specimen cracked almost immediately upon upon flame ignition; white coating did form on main portion of specimen
HF-126	Al_2O_3	1700 1910 2150 2280 2150 1910 1700	1 0.58 0.58 2.08 0.67 0.58 1.0	1254	2.4	0	3.7 Average	0.48 Average	Specimen corroded unevenly
HF-128	Al_2O_3	1700 1910 2150 2280 2150 1910 1700	1.0 0.58 0.58 2.67 0.58 0.58 1.0	1514	11.7	2.2-1.7	8.3 Average	1.1 Average	Flame apparently off-center; uneven corrosion; visible crack lines
HF-130	Al_2O_3	1700 1900 1700	1.0 7.25 1.0	1048[a]	0.07	0	0	0	Thermocouple experiment
HF-131	Al_2O_3 HF-130	1700 2000 1700	1.0 8.0 1.0	1095[a]	0.39	0	0.2	0.03	Thermocouple experiment. Several whiskers appeared at top outer edge

[a] Highest thermocouple reading in center of specimen at point nearest the top surface

Run No.	Material	Theoretical Flame Temperature (K)	Duration of Run (min)	Sample Surface Temperature (K)	Weight Loss (%)	Diameter Loss (%)	Height Loss (%)	Measured Loss in Height (mm)	Remarks
HF-132	Al$_2$O$_3$ HF-131	1700 2090 2215 1700	1.0 8.33 3.95 1.0	1325	5.99	1.4	10.1 (max.)	1.3 (max.)	Thermocouple experiment Two-thirds of top surface was corroded; center thermocouple hole became visible, some cracks observed
HF-133	BeO National	1700 1830 2215 2395 1830 1700	1.0 1.0 6.33 3.33 1.0 1.0	1315	53.3	12.4 Average	32.6 Average	3.2	Specimen corroded
HF-134	BeO (Y-12)	1700 1830 2215 1830 1700	1.0 1.0 3.17 1.0 1.0	1267	18.6	2.8 Average	10.3 Average	1.2 Average	Specimen corroded; stuck to support due to melting
HF-135	Al$_2$O$_3$	1700 1910 2150 2280 2150 1910 1700	1.0 0.58 0.58 4.58 0.58 0.58 1.0	1446	17.6	4.0 Average	8.1 Average	1.0 Average	Specimen corroded unevenly
HF-137	Single Crystal MgO	1700 1830 2450 1830 1700	1.0 1.0 2.5 1.0 1.0	1692	NA	+0.9	9.9	1.3	Specimen melted on top and cracks developed

EXTERNAL DISTRIBUTION

SAMSO
Attention: Lt. Col. J. R. Doughty
Worldway Postal Center
Post Office Box 92960
Los Angeles, CA 90009

Rocket Propulsion Laboratory
Attention: Maj. John Dean
Edwards Air Force Base, CA

TRW/DSSG
Attention: Dr. Richard Ackerman
           Dr. Joe Mace
Mail Station 01/2270
One Space Park
Redondo Beach, CA   90278

Rocketdyne
Attention: Dr. H. Carpenter
Dept. 590-175/B 833
M.C. BAO-4
6633 Canoga Park, CA 91304

Air Force Weapons Laboratory
Attention: Capt. N. Pchelkin
           Capt. Paul Flynn
           Maj. D. Olson
Kirtland Air Force Base, N. M. 87117

Air Force Materials Laboratory
Attention: Dr. H. Graham
Wright-Patterson Air Force Base, Ohio 45433

Los Alamos Scientific Laboratory
Attention: Dr. Roy Feber, CMB-8
           Dr. Steven Stoddard, CMB-6
           Dr. Terry Wallace, CMB-3
           Dr. D. J. Sandstrom, CMB-6
           Dr. P. Wagner, CMB-8
Los Alamos, New Mexico 87544

Bell Aerospace Company
Attention: Dr. Wayne Solomon
           Dr. Frank Anthony
Post Office Box One
Buffalo, N. Y.   14240

Atlantic Research Corporation
Attention: J. R. MacPherson
5390 Cherokee Avenue
Alexandria, VA   22314

Yale University
Attention: Prof. Paul C. Nordine
Department of Engineering and Applied Science
Chemical Engineering Section
New Haven, CT   06520

U. S. Army Research Office
Post Office Box 12211
Research Triangle Park, North Carolina   27709

DARPA/Materials Sciences
Attention: Dr. Arden Bement
             Capt. Harry Winsor
             Dr. Stanley Ruby
1400 Wilson Blvd.
Arlington, VA   22209

Rice University
Department of Chemistry
Attention: Dean John L. Margrave
Post Office Box 1892
Houston, Texas   77001

United Technologies Research Center
Attention: Mr. Ronald Grose
            Mr. Arthur Chalfante
East Hartford, Conn.   06108

Lawrence Livermore Laboratory
Attention: Dr. Don Olander
Post Office Box 808
Livermore, California 94550

Stanford Research Institute
Attention: Dr. D. L. Hildenbrand
333 Ravenswood Avenue
Menlow Park, CA   94025

U. S. Army Missile Research and Development Command
DRDMI-HAL
Attention: J. Walters
            S. Clapp
Redstone Arsenal, AL   35809

INTERNAL DISTRIBUTION

H. D. Hickman

E. J. Barber, ORGDP

D. J. Bostock

J. M. Case

R. L. Farrar, ORGDP

C. F. Hale, ORGDP

C. E. Holcombe

L. Kovach

G. B. Marrow

J. M. Mills/TIC

J. H. Pashley, ORGDP

L. R. Phillips

A. J. Taylor

W. H. Thompson, Jr./F. D. Bender

P. R. Vanstrum

G. W. Weber

W. J. Wilcox, Jr.

W. R. Martin

Y-12 Central Files (Y-12RC)